Journal of Computational and Applied Mathematics 227 (2009) 294–307

Contents lists available at ScienceDirect

Journal of Computational and Applied Mathematics

journal homepage: www.elsevier.com/locate/cam

Wavelet-based fingerprint image retrieval

Javier A. Montoya Zegarra [a,b,*], Neucimar J. Leite [b], Ricardo da Silva Torres [b]

[a] Computer Engineering Department, Faculty of Engineering, San Pablo Catholic University, Av. Salaverry 301, Vallecito, Arequipa, Peru
[b] Institute of Computing, University of Campinas, Av. Albert Einstein, 1251, CEP 13084-851, Campinas, SP, Brazil

ARTICLE INFO

Article history:
Received 4 April 2006
Received in revised form 30 September 2007

Keywords:
Wavelets
Content-based image retrieval
Texture image retrieval
Fingerprints

ABSTRACT

This paper presents a novel approach for personal identification based on a wavelet-based fingerprint retrieval system which encompasses three image retrieval tasks, namely, feature extraction, similarity measurement, and feature indexing.

We propose the use of different types of Wavelets for representing and describing the textural information presented in fingerprint images in a compact way. For that purpose, the feature vectors used to characterize the fingerprints are obtained by computing the mean and the standard deviation of the decomposed images in the wavelet domain. These feature vectors are used both to retrieve the most similar fingerprints, given a query image, and their indexation is used to reduce the search spaces of candidate images. The different types of Wavelets used in our study include: Gabor wavelets, tree-structured wavelet decomposition using both orthogonal and bi-orthogonal filter banks, as well as the steerable wavelets.

To evaluate the retrieval accuracy of the proposed approach, a total number of eight different data sets were considered. We also took into account different combinations of the above wavelets with six similarity measures. The results show that the Gabor wavelets combined with the Square Chord similarity measure achieves the best retrieval effectiveness.

1. Introduction

Biometrics, which refers to the automatic recognition of individuals by their physical and/or behavioral characteristics, has emerged as a motivating and instigating research field [1]. In fact, several biometric applications have been adopted in civilian, commercial, and forensic areas. Traditionally, the physical characteristics used for human recognition include fingerprints [2], iris [3], retinal [4], and facial [5], while the behavioral ones include signature [6], voice [7], and gait [8]. Among all these biometric characteristics, fingerprints are considered one of the most reliable for human recognition due to their individuality and persistence [9]. The fingerprint's individuality means that it is unique across individuals and across fingers of the same individual, even in identical twins [10]. On the other hand, the fingerprint's persistence means that the basic fingerprint characteristics do not change with time.

The popularity of fingerprint-based recognition has led to the creation of large-scale databases. While the large size of these collections compromises the retrieval speed, the noise and the distortion that can be found in fingerprint images may reduce the overall retrieval accuracy. Therefore, both retrieval accuracy and speed play an important role in the fingerprint recognition process.

* Corresponding author at: Computer Engineering Department, Faculty of Engineering, San Pablo Catholic University, Av. Salaverry 301, Vallecito, Arequipa, Peru.
E-mail addresses: javier.montoya@ic.unicamp.br (J.A. Montoya Zegarra), neucimar@ic.unicamp.br (N.J. Leite), rtorres@ic.unicamp.br (R. da Silva Torres).

0377-0427/$ – see front matter © 2008 Elsevier B.V. All rights reserved.
doi:10.1016/j.cam.2008.03.017

Automatic fingerprint recognition often involves four steps [2,11]: (1) acquisition, (2) classification, (3) identification, and (4) verification. Fingerprint acquisition refers to the capture and representation of fingerprints. Fingerprint classification consists in assigning a fingerprint to a pre-defined class, whereas fingerprint identification is referred to the retrieval of fingerprints that corresponds to a given fingerprint query image (one-to-many comparisons). Finally, fingerprint verification is used to determine whether two fingerprint images are the same or not (one-to-one comparisons). However, considering the large size of the fingerprint image databases and the computational cost of fingerprint verification algorithms, it is necessary to reduce the number of one-to-one comparisons during fingerprint verification, seeking improvements both in accuracy and retrieval speed.

In this sense, we propose an original approach to guide the search and retrieval in fingerprint image databases. More particularly, we study the textural patterns that can be found in the central region of fingerprints in order to generate textural feature vectors used for fingerprint indexing and retrieval. For that purpose, we exploit the capability of different types of well-known wavelet transforms to integrate both multiresolution and space-frequency properties in a natural manner. The fingerprint images are then decomposed into different spatial/frequency subimages and some statistical analyses are performed to generate feature vectors. These feature vectors are then used to compare the similarity among a given fingerprint query image and the database images.

In our approach, the texture features are extracted by different types of the wavelet transforms which include steerable wavelet (known as Steerable Pyramid [12]), Gabor Wavelet Transform (GWT [13,14]), Tree-Structured Wavelet Decomposition using orthogonal filter bank (TSWD Haar, Daubechies 4-, 8-, and 16-Tap [15,16]), and Tree-Structured Wavelet Decomposition using bi-orthogonal filter bank (spline wavelets [17]).

For the Steerable Pyramid, different orientation filters and decomposition levels are used to generate a translation- and rotation-invariant fingerprint representation. In the GWT, different scales and orientations are used to capture the relevant texture information, whereas in the TSWD, the image texture content is captured on the low frequency sub-band, while the high frequency sub-band is used to capture the image variations in different directions.

The focus of our work is to illustrate the utility and suitability of applying different types of wavelet transforms for fingerprint indexing and retrieval. To the best of our knowledge, this work represents the first attempt to characterize the textural content of fingerprint images by using this kind of image transformation. In this context, the main contributions of this paper are:

(1) a description of a texture-based retrieval system for fingerprint identification considering both feature extraction methods and similarity measures.
(2) the treatment of the fingerprint identification problem as a wavelet-based image retrieval challenge.
(3) a detailed comparison of the retrieval accuracy achieved by different combinations of types of wavelet transforms and similarity measures in terms of precision and recall curves.
(4) the validation of the suitability of the wavelet transforms to represent and describe the fingerprint characteristics.

The remainder of this paper is organized as follows. The next section summarizes some related concepts, whilst Section 3 presents an overview of related works and outlines the context of our study. Section 4 describes the architecture of the proposed system. The module used for detecting the center point region of the fingerprints is presented in Section 5. Various wavelet-based feature extraction algorithms are described in Section 6. The feature representation for each type of wavelet is presented in Section 7. Different similarity metrics and the feature indexing method are described in Section 8. The results of our experiments are discussed in Section 9. Finally, our conclusions are drawn in Section 10.

2. Background

In this section, we formalize the main terms used along this paper.

2.1. Image descriptors

Definition 1. An **image descriptor** D is defined as a pair (ϵ_D, δ_D), where $\epsilon_D : I \to \mathbb{R}^n$ is a function that extracts a feature vector $\vec{v}_I$ from a given image I, and $\delta_D : \mathbb{R}^n \times \mathbb{R}^n \to \mathbb{R}^n$ denotes the distance function used to compute similarity between two images considering their feature vectors. The smaller the distance, the more similar the images.

Definition 2. A **feature vector** $\vec{v}_I$ of an image I is a point in $\mathbb{R}^n$ space, such that: $\vec{v}_I = (v_1, v_2, \ldots, v_n)$, where n denotes the dimension of the vector.

2.2. Metric spaces

Definition 3. A **metric distance** function $d()$ is a function that has the following properties:

(i) Symmetry: $d(O_1, O_2) = d(O_2, O_1)$
(ii) Positiveness: $0 < d(O_1, O_2) < \infty$, $O_1 \neq O_2$ and $d(O_1, O_2) = 0$

(iii) Triangle inequality: $d(O_1, O_3) \leq d(O_1, O_2) + d(O_2, O_3)$

where O denotes the domain of a set of objects $O = (O_1, O_2, \ldots, O_n)$. The pair (O, d) is known as **metric space**. The similarity functions of the image descriptors are special cases of metric spaces.

Definition 4. A **Metric Access Methods** (MAM) is a class of Access Method (AM) that is used to manage large volumes of metric data allowing insertions, deletions and searches [18].

2.3. Similarity queries

In metric spaces two well-known similarity queries that can be performed are:

Definition 5. Given the query object O_q and the maximum search distance r_q, the **range query** $R_q(O_q, r_q)$ is used to retrieve all the objects $O_r \in O$ that satisfy the following condition: $d(O_q, O_r) < r_q$.

Definition 6. Given the query object O_q and the value $k \in Z^+$, the **k-Nearest Neighbor Query** ($kNN(O_q, k)$) retrieve the k-closest objects in $O_r \in O$ that satisfy the following properties: $|O_r| = k$ and $d(O_q, O_r) \leq d(O_q, O_s) \forall O_s \in O$.

3. Related work

The most common way to reduce the number of one-to-many comparisons, during fingerprint retrieval, is to partition the database using fingerprint classification techniques which can be divided into two main categories: exclusive and continuous classification.

The former uses information related to the pattern of ridges and valleys found in fingerprints to partition the fingerprint database into mutual exclusive bins. In this sense, once the fingerprint query image is classified, the image candidates are searched in the corresponding bin. Further, this kind of approach can be subdivided into four subcategories depending on the type of information used for exclusive classification, namely, ridge-, orientation field-, singularity-, and structural-based information. In continuous classification approaches, fingerprint images are represented by feature vectors. Similarities among fingerprint images are established by the distance in the feature space of their corresponding feature vectors. This approach is closely related to a fingerprint database indexing problem.

Ridge-based approaches traditionally use the information of the structure frequency of the fingerprint ridges for classification purposes. The work proposed by Fitz et al. [19] takes into account the frequency spectrum of fingerprints, obtained by applying a hexagonal Fourier Transform, to classify fingerprints into three classes: whorls, loops, and arches. A wedge-ring detector is used to partition the frequency domain images into non-overlapping areas in which the pixel values are summed up to form a feature vector. Once the feature vector is found, it is compared to the reference feature vectors of each of the classes and a further classification is performed by using a nearest neighbor classification method. To capture the structure of fingerprint ridges, some works develop mathematical models to characterize the corresponding images [20,21]. Chong et al. [21] use, for example, B-splines curves to approximate the shape of the fingerprint ridges. Then, similar orientation ridges are grouped together to obtain a global shape representation of the fingerprints which is used for classification.

Approaches based on orientation fields use the local average orientations of fingerprint ridges to classify fingerprints. Halici et al. [22] use the block orientation fields of fingerprints and certainty measures to generate the fingerprint feature vectors. For the sake of feature dimensionality reduction, they consider a SOM neuronal network to improve the overall classification accuracy.

Fingerprint singularities have been widely used for classification [23,24]. They can be defined as the local regions where the fingerprint ridges present some physical properties. Karu et al. [24] extract the singularities that can be found in the fingerprints to classify them by considering the location and the number of the detected singularities.

Structural approaches use the topology information of fingerprints for classification purposes. Maio et al. [25] segment the orientational field of fingerprint images to represent the fingerprints as relational graphs. For each class of fingerprints, a relational graph model is created. An inexact graph matching algorithm is used to classify fingerprint images.

Although the search spaces can be reduced in exclusive classification approaches, there are some shortcomings that should be considered: (1) some fingerprints present properties of more than one class and therefore they cannot be assigned to just one bin, (2) natural distribution of fingerprints is not uniform and therefore, even by performing binning in the original database, the number of one-to-many comparisons can still be high – Cappelli et al. [26] proved that the distribution of fingerprint classes is not uniform (93.4% of fingerprints are among a set of three classes) –, and (3) some of the characteristics used for binning are not easy to detect due to the presence of noise, ambient conditions, etc.

On the other hand, Germain et al. [27] proposed a continuous system to index fingerprint databases using flash hashing. For that purpose, the location and orientation of the minutiae, as well as the number of ridges among them, are used to generate feature vectors. Some information related to the feature vectors are obtained and used to create the image indices that are added to a multi map memory structure and considered later during the fingerprint retrieval.

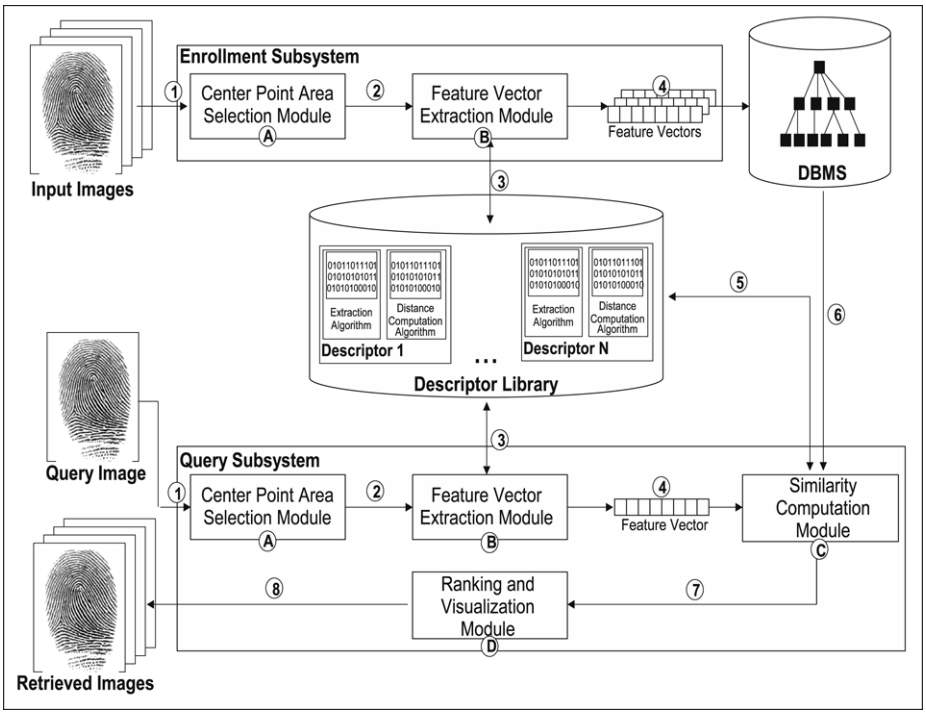

Fig. 1. Architecture of the proposed system.

More recently, Tan et al. [28] compared two fingerprint identification approaches based on: (a) classification followed by verification, and (b) indexing followed by verification. Their classification method uses genetic programming to generate composite operators applied to some features extracted from the fingerprint orientation fields. A Bayesian classifier is then used to classify the images. Their indexing approach is based on the work by Germain [27]. However, as a result of the retrieval process, a list of N fingerprint candidates is retrieved and the verification process determines the correspondence degree between the query image and the database ones. They concluded that the indexing-based approach outperforms the classification method if we take into account the size of the search spaces.

The above mentioned approaches reduce the search spaces by considering some fingerprint singularities [27,28]. Furthermore, the accurate detection of these singularities depends highly on the quality of the fingerprint images. Moreover, their definition often involves high computational costs that will affect directly the fingerprint recognition time. On the other hand, they both consider flash hashing for indexing purposes and we believe that by using metric access methods the query processing time can be improved. In this work, we will consider more specifically the textural information presented in fingerprints for feature extraction purposes, since it retains the discriminating power of fingerprints and can be directly associated to Metric Access Methods (MAM) for the data indexing. The description of the MAM used in our approach is beyond the scope of this paper, however a brief description of such a method is given in Section 8.

4. System overview

The architecture of our proposed framework, presented in Fig. 1, can be divided into two main subsystems, namely, the enrollment and the query subsystems. The enrollment subsystem acquires the information stored in the database for later use. The query subsystem is responsible for retrieving similar fingerprints from the database according to the user's fingerprint query image. Our system operates as follows:

(1) Enrollment-subsystem: several fingerprint images are first captured (arrow labeled 1 in Fig. 1) and a Region of Interest (ROI) within the fingerprint is marked (module 1, arrow 2) by a center point area detection module. A region of 64×64 pixels is used for marking the ROI. Feature extraction algorithms contained in the descriptor library (module B, arrow 3) are used by the feature extraction module to generate the features (arrow 4) which are indexed by a metric access method for further use.

(2) Query-subsystem: a fingerprint query image is received as input from the user (arrow 1). Once the fingerprint ROI is detected (module A, arrow 2), the feature extraction algorithms contained in the descriptor library are used to extract the feature vectors from the query image (module B with arrows 3 and 4, respectively). The query image feature vector is used to rank the database images according to their similarity to the query image (module C). For that purpose, a distance computation algorithm is selected from the descriptor library (arrow 5) and the metric access method is used

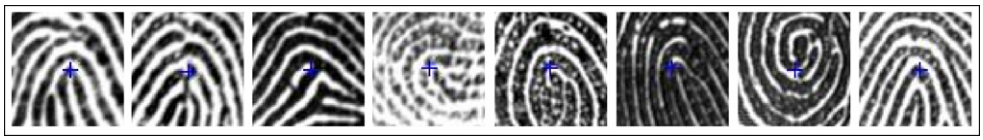

Fig. 2. Some center point areas detected from 8 different fingerprints contained in the FVC-2002 Database.

to speed up the retrieval process (arrow 6). Finally, the most similar database images are ranked (arrow 7) and returned to the user (arrow 8).

5. Center point area detection

In order to detect the fingerprint center point area, we first locate the core point corresponding to the uppermost point contained in the inner-most ridge line. We have chosen the core point as the basis for the center area detection because: (1) it can be found in the central part of the fingerprint and, (2) it appears more frequently than deltas [29]. The steps used for core detection are [30]:

(1) Estimation and smoothing of the directional fields of the fingerprint input image.
(2) Computation of the Poincaré index, in each (8×8) block. This index is defined as follows:

$$\text{Poincare}(i,j) = \frac{1}{2\pi}\sum_{k=0}^{N-1} \Delta(k) \tag{1}$$

$$\Delta(k) = \begin{cases} \delta(k) & \text{if } |\delta(k)| < \dfrac{\pi}{2} \\ \pi + \delta(k) & \text{if } \delta(k) \leq -\dfrac{\pi}{2} \\ \pi - \delta(k) & \text{otherwise.} \end{cases} \tag{2}$$

$$\delta(k) = \theta(X(k'), Y(k')) - \theta(X(k), Y(k)) \tag{3}$$

where $k' = (k+1) \bmod (N)$ and $\theta(i,j)$ is the directional field of the fingerprint image. $X(k)$ and $Y(k)$ are the coordinates of the blocks in the closed curve with N blocks. If the Poincaré index has a value of $1/2$, then the current block is the core block. The center of this block is then the core point. If more than two cores are detected, go back to step 1 using a larger smoothing parameter for the directional fields.

Once the center point is obtained, a center point area can be easily defined. An image of size 64×64 pixels around the core point is then cropped, as shown in Fig. 2.

6. Feature extraction

In this section, we provide a more detailed explanation of the various wavelet-based feature functions considered in the feature extraction module of the proposed architecture (See Fig. 1, Module B). Wavelets have proved their efficiency in image retrieval problems due to their capability in capturing both texture and shape information [31,32]. The wavelet sub-band and multi-resolution decomposition are extremely adapted to compute relevant information of the data while preserving their basic content [33]. In this section, we present the wavelet-based feature extraction approaches considered in our system.

6.1. Texture feature extraction

The texture found in images represents a powerful discriminating feature for both image classification and retrieval. Although there does not exist a formal definition of texture, it can be understood as the basic primitives in images whose spatial distribution creates some visual patterns. Thus, the goal of a texture feature extraction method is to create a feature vector that captures the image texture information while preserving its content.

By considering that the ridges and valleys of fingerprints form a textural pattern, it is then possible to capture discriminatory information through their textural representations. Further, the captured representations in the feature vectors can be indexed and stored for image retrieval purposes.

6.2. Wavelet-based feature extraction

Here, the use of the wavelet transforms for texture description is motivated by two reasons [31]: (1) it integrates both multiresolution and space-frequency properties naturally, and (2) it has demonstrated good accuracy for texture analysis and classification.

6.2.1. Wavelet transform review

A wavelet transform decomposes a signal $f(x)$ with a family of functions obtained through dilations and translations of a kernel function $\psi(x)$, called the mother wavelet. It is localized in both spatial and frequency domains. This family of functions is denoted by:

$$\psi_{m,n}(x) = 2^{\frac{-m}{2}}\psi(2^m x - n) \tag{4}$$

where $m, n \in \mathbb{Z}^+$ indicate dilations and translations, respectively. To construct the mother wavelet $\psi(x)$ a scaling function $\phi(x)$ is needed:

$$\phi(x) = \sqrt{2}\sum_k h(k)\phi(2x-k). \tag{5}$$

Then, the wavelet kernel $\psi(x)$ is determined as follows:

$$\psi(x) = \sqrt{2}\sum_k g(k)\phi(2x-k) \tag{6}$$

with

$$g(k) = (-1)^k h(N-1-k), \tag{7}$$

where N is the support of the digital filter. The explicit forms of $\phi(x)$ and $\psi(x)$ are not required to perform the wavelet transform because it depends only on the coefficients $h(k)$ and $g(k)$ with low- and high-pass characteristics, respectively. The L-level decomposition of the signal $f(x)$ can be written as:

$$\begin{aligned} f(x) &= \sum_n c_{0,n}\phi_{0,n}(x) \\ f(x) &= \sum_n c_{L,n}\phi_{L,n}(x) + \sum_{l=1}^{L+1}\sum_n d_{l,n}\phi_{l,n}(k) \end{aligned} \tag{8}$$

the coefficients $c_{0,n}$ are given and the coefficients $c_{L,n}$ and $d_{l,n}$, both at scale l, are obtained by the coefficients $c_{l-1,n}$ at scale $l-1$ through:

$$\begin{aligned} c_{l,n} &= \sum_k c_{l-1,n}h(k-2n) \\ d_{l,n} &= \sum_k c_{l-1,n}g(k-2n) \end{aligned} \tag{9}$$

where $1 \le l \le L+1$. A recursive wavelet decomposition can be obtained through $h(k)$ and $g(k)$ in Eq. (9). The same process can be viewed as the convolution of signal $c_{l-1,n}$ with the impulse responses $\overline{h(n)} = h(-n)$ and $\overline{g(n)} = g(-n)$ of the low- and high-pass filters H and G, respectively (also known as quadrature filters), and then by downsampling the filtered signals by a factor of 2. The 2-D wavelet and scaling functions can be expressed as the tensor products of their 1-D complements:

$$\begin{aligned} \phi_{LL}(x,y) &= \phi(x)\phi(y) \qquad \psi_{LH}(x,y) = \phi(x)\psi(y) \\ \psi_{HL}(x,y) &= \psi(x)\phi(y) \qquad \psi_{HH}(x,y) = \psi(x)\psi(y) \end{aligned} \tag{10}$$

where ϕ_{LL}, ψ_{LH}, ψ_{HL}, and ψ_{HH} represent the Low-Low, Low-High, High-Low, and High-High sub-bands, respectively.

6.2.2. Tree-structured wavelet transform

In the Tree-Structured Wavelet Transform, the output of each of the sub-bands (ϕ_{LL}, ψ_{LH}, ψ_{HL}, ψ_{HH}) can be decomposed recursively. This decomposition is based on the fact that, for some kinds of textures, the most relevant information can be found in the middle sub-bands. To avoid a full decomposition, Chang et al. [34] proposed an energy-based criterion to decide which sub-band should be further decomposed. If the energy in a sub-band is very similar to the maximum energy of a sub-band at the same level, then further decomposition is not performed. However, for the sake of pattern retrieval, a fixed decomposition structure is convenient, since if facilitates distance computations and hence database browsing. On the other hand, by considering that the sub-band ψ_{HH} often leads to unstable features, recursively decomposition is done in the ϕ_{LL}, ψ_{LH}, and ψ_{HL} sub-bands.

For the Tree-Structured Wavelet Decomposition, we have considered two kinds of filter banks, which include orthogonal and bi-orthogonal filter banks. For the orthogonal filter bank we used the Haar wavelets, and Daubechies 4-, 8-, and 16-tap [15,16]. For the bi-orthogonal filter bank the spline wavelets are used [17]. Fig. 3 presents an example of a two level Tree-Structured Wavelet Transform Decomposition for image retrieval. Note that the ψ_{HH} sub-band is not further decomposed for the reasons explained above.

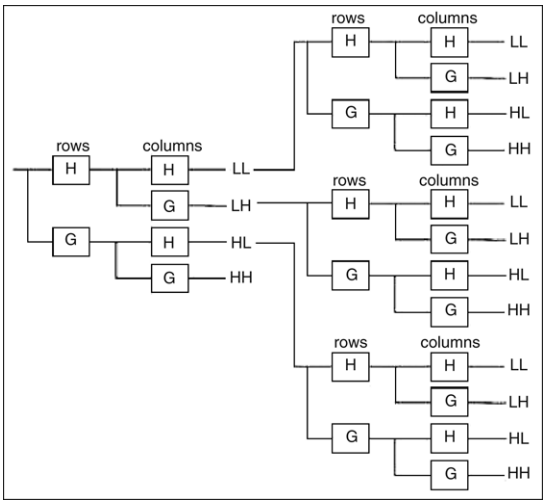

Fig. 3. Two level tree-structured wavelet transform.

6.2.3. Gabor wavelet transform

A general 2-D Gabor function $\psi(x, y)$ is defined as:

$$\psi(x, y) = \left(\frac{1}{2\pi\sigma_x\sigma_y}\right) \exp\left[-\frac{1}{2}\left(\frac{x^2}{\sigma_x^2} + \frac{y^2}{\sigma_y^2}\right) + 2\pi jWx\right] \tag{11}$$

where the spatial coordinates (x, y) denote the centroid localization of the elliptical Gaussian window. The parameters σ_x and σ_y are the space constants of the Gaussian envelope along the x- and y-axes, respectively. The Fourier transform $G(u, v)$ of the Gabor function $\psi(x, y)$ can be written as:

$$G(u, v) = \exp\left[\frac{-1}{2}\left(\frac{(u - W)^2}{\sigma_u^2} + \frac{v^2}{\sigma_v^2}\right)\right] \tag{12}$$

where W represents the frequency of the sinusoidal plane along the horizontal axis and the frequency components in x- and y-direction are denoted by the pair (u, v), while $\sigma_u = 1/2\pi\sigma_x$ and $\sigma_v = 1/2\pi\sigma_y$. Considering the non-orthogonal basis set formed by the Gabor functions, a localized frequency description can be obtained by expanding a signal with this basis.

Self-similar class functions, known as Gabor wavelets, can be generated by dilations and rotations of the mother wavelet $\psi(x, y)$, i.e.:

$$\psi_{m,n}(x, y) = a^m \psi_{x',y'}, \quad a > 1 \tag{13}$$

considering $m = 1, \ldots S$ and $n = 1, \ldots K$. S and K denote the total number of dilations and orientations, respectively, and:

$$\begin{bmatrix} x' \\ y' \end{bmatrix} = a^{-m} \begin{bmatrix} \cos\theta_n & \sin\theta_n \\ -\sin\theta_n & \cos\theta_n \end{bmatrix} \begin{bmatrix} x \\ y \end{bmatrix} \tag{14}$$

where $\theta = n\pi/K$ and θ is the rotation angle. To ensure that the energy is independent of m, a scale factor a^{-m} is introduced. Considering the redundant information presented in the filtered images due to the non-orthogonality of the Gabor wavelets, Manjunath et al. [14] designed a strategy to reduce the redundancy of the Gabor wavelets filter bank, where the half-peak magnitude of the filter responses touches each other in the frequency spectrum:

$$a = \left(\frac{U_h}{U_l}\right)^{\frac{1}{S-1}} \qquad \sigma_u = \frac{(a - 1)U_h}{(a + 1)\sqrt{2\ln 2}} \tag{15}$$

$$\sigma_v = \tan\left(\frac{\pi}{2K}\right)\left[U_h - 2\ln 2\left(\frac{\sigma_u^2}{U_h}\right)\right]\left[2\ln 2 - \frac{(2\ln 2)^2\sigma_u^2}{U_h^2}\right]^{-\frac{1}{2}} \tag{16}$$

where $W = U_h$. The parameters U_h and U_l are used, respectively, to denote the upper and lower center frequencies of interest.

6.2.4. Steerable pyramid

The Steerable Pyramid is a linear multi-orientation and multi-scale image decomposition method from which an image is subdivided into a collection of sub-bands, localized at different scales and orientations [12]. This decomposition is based on convolution and decimating operations and has the advantage that the sub-bands are translation- and rotation-invariant.

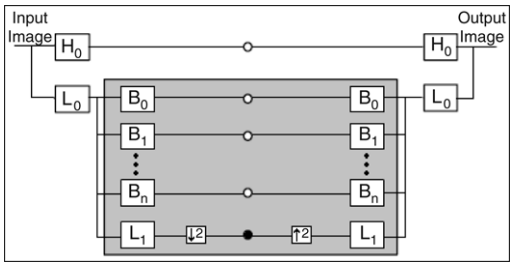

Fig. 4. First level of steerable pyramid decomposition.

Using a high- and low-pass filter (H_0, L_0) the input image is initially decomposed into high- and low-pass sub-bands. The low-pass sub-band is further decomposed into a total of k-oriented band-pass portions $B_0, \ldots, B_k$ and into a low-pass sub-band L_1. The recursive decomposition is done by subsampling by a factor of 2 along the rows and columns the lower low-pass sub-band. The decomposition process of the first level of the Steerable Pyramid is shown in Fig. 4. The white points in Fig. 4 represent the resulting images after applying the directional filters on the input images, whereas the black point denotes the recursive pyramidal decomposition.

7. Feature representation

The way the feature vectors are computed, based on the different types of Wavelets presented in Section 6, is described in this section (See Fig. 1, arrow 4). Here, some statistical measures are used to generate the feature vectors. More precisely, the mean μ_{mn} and the standard deviation σ_{mn} of the energy distribution of the multiresolution transform coefficients are used to capture the fingerprint textural information and, thus, to form the feature vector $\vec{f}$:

$$\mu_{mn} = \frac{1}{MN} \iint |W_{mn}(x, y)| \, \mathrm{d}x\mathrm{d}y \tag{17}$$

$$\sigma_{mn} = \sqrt{\iint (W_{mn}(x, y) - \mu_{mn})^2 \, \mathrm{d}x\mathrm{d}y}. \tag{18}$$

For the Tree-Structured Wavelet Transform the values of $|W_{mn}(x, y)|$ correspond to the energy distribution in one of the three sub-bands: LL, LH, and HL. Thus, the subindices m and n are integers that stand for the decomposition level and the current sub-band ($m = 1, 2, \ldots, L$ and $n = 1, 2, 3$), respectively. Furthermore, the 64×64 cropped image is decomposed into 6 levels, thus a total number of 18 sub-bands are considered. The feature vector $\vec{f}$ is formed as follows:

$$\vec{f_{TSWT}} = [\mu_{11}, \sigma_{11}, \mu_{12}, \sigma_{12}, \mu_{13}, \sigma_{13}; \ldots; \mu_{L1}, \sigma_{L1}, \mu_{L2}, \sigma_{L2}, \mu_{L3}, \sigma_{L3}]. \tag{19}$$

For the Gabor Wavelet Transform, the values of $|W_{mn}(x, y)|$ denote the energy distribution of the transform coefficients after convolving an image I with the Gabor wavelet $\psi_{m,n}$. By considering a total number of $S = 6$ scales and $K = 16$ orientations, the resulting feature vector is computed as follows:

$$\vec{f}_{GW} = [\mu_{11}, \sigma_{11}; \mu_{12}, \sigma_{12}; \ldots \mu_{SK}, \sigma_{SK}]. \tag{20}$$

For $k = 16$ orientation sub-bands and $l = 6$ decomposition levels, the feature vector for the case of the Steerable Pyramid is generated as follows:

$$\vec{f_{SP}} = [\mu_{11}, \sigma_{11}, \mu_{21}, \sigma_{21}, \ldots, \mu_{k1}, \sigma_{k1}, \mu_{1l}, \sigma_{1l}, \mu_{2l}, \sigma_{2l}, \ldots, \mu_{kl}, \sigma_{kl}]. \tag{21}$$

8. Feature indexing

In this section, we present the different similarity measures studied in our work and the MAM used for feature indexing.

8.1. Similarity measures

The similarity measure functions used for computing the similarity among images are a key component of a CBIR (Content-based image retrieval)system. This affirmation is valid if we consider that the retrieval performance depends not only on the effectiveness of the image features, but also on the similarity measures efficiency. Thus, different similarity measures should be analyzed in a CBIR system to improve the retrieval performance. Let $\vec{x} = (x_1, x_2, \ldots, x_n)$ and $\vec{y} = (y_1, y_2, \ldots, y_n)$ be two feature vectors of dimension n, Table 1 presents the similarity measures considered in this work.

Table 1
Evaluated similarity measures

Evaluated similarity measures	
Measure	Formula
Bray Curtis	$d_{BC} = \sum_{i=1}^{n} \frac{\lvert x_i - y_i \rvert}{x_i + y_i}$
Canberra	$d_C = \sum_{i=1}^{n} \frac{\lvert x_i - y_i \rvert}{\lvert x_i \rvert + \lvert y_i \rvert}$
Euclidean	$d_E = \sqrt{\sum_{i=1}^{n} (x_i - y_i)^2}$
Manhattan	$d_M = \sqrt{\sum_{i=1}^{n} \lvert x_i - y_i \rvert}$
Squared Chord	$d_{SC} = \sum_{i=1}^{n} \left(\sqrt{x_i} - \sqrt{y_i}\right)^2$
Square Chi-Squared	$d_{SChi} = \sum_{i=1}^{n} \frac{(x_i - y_i)^2}{x_i + y_i}$

Table 2
Summarization of the FVC-2002, and FVC-2004 databases

	Technology	Scanner	Image Size	Resolution
	FVC-2002			
DB1	Optical sensor	Indentix TouchView II	388 × 374	500 dpi
DB2	Optical sensor	Biometrika FX 2000	296 × 560	569 dpi
DB3	Capacitive sensor	Precise Biometrics 100SC	300 × 300	500 dpi
DB4	Synthetic software	SFingGE v2.51	288 × 384	About 500 dpi
	FVC-2004			
DB1	Optical sensor	CrossMatch v300	640 × 480	500 dpi
DB2	Optical sensor	Digital Persona U.are U.400	328 × 364	500 dpi
DB3	Thermal Sweeping sensor	Atmel FingerChip	300 × 480	512 dpi
DB4	Synthetic software	SFingGE v3.0	288 × 384	About 500 dpi

8.2. Metric access methods

To speed-up the retrieval, we have used a dynamic MAM known as Slim-tree [18]. The use of the Slim-tree in the fingerprint domain is attractive, since: (1) fingerprints can be inserted and deleted even after the creation of the tree, due to its dynamicity, (2) similarity queries such as kNN and range queries are supported which allows CBIR applications, (3) overlapping between nodes is minimized and thus the retrieval speed is increased, and (4) due to its scalability, large amounts of data can be handled in an efficient manner, even after an increase of the database. Furthermore, the Slim-tree has outperformed the well-known M-tree indexing structure [35].

9. Experimental results

In this section, we present the experimental setup conducted in our study, as well as the effectiveness of the discussed feature extraction methods by means of some precision vs. recall curves.

9.1. Databases

Our experiments were conducted independently on two databases, the Bologna FVC-2002, and FVC-2004 databases, which consist of four different data sets, referred to as DB1, DB2, DB3, and DB4. Further, each of these data sets contains 8 fingerprint samples of 100 different fingers. Thus, each data set has 880 fingerprints. By considering that each data set was collected through different fingerprint technologies, in order to cover the advances in fingerprint sensing techniques, the size of the fingerprint images, as well as the resolution, varies among them. Data sets DB1, DB2, and DB3 were collected by different scanners technologies, whereas the data set DB4 was collected by using a software for generating synthetic fingerprints [36,37]. Table 2 summarizes the different fingerprint technologies used to generate the databases.

These databases were not acquired in real environments and, according to a formal protocol, the data are characterized by the presence of distortions (rotations, translations, low quality images) within fingerprints of the same individual's finger. All these aspects make these data sets very useful for testing our system in extreme conditions.

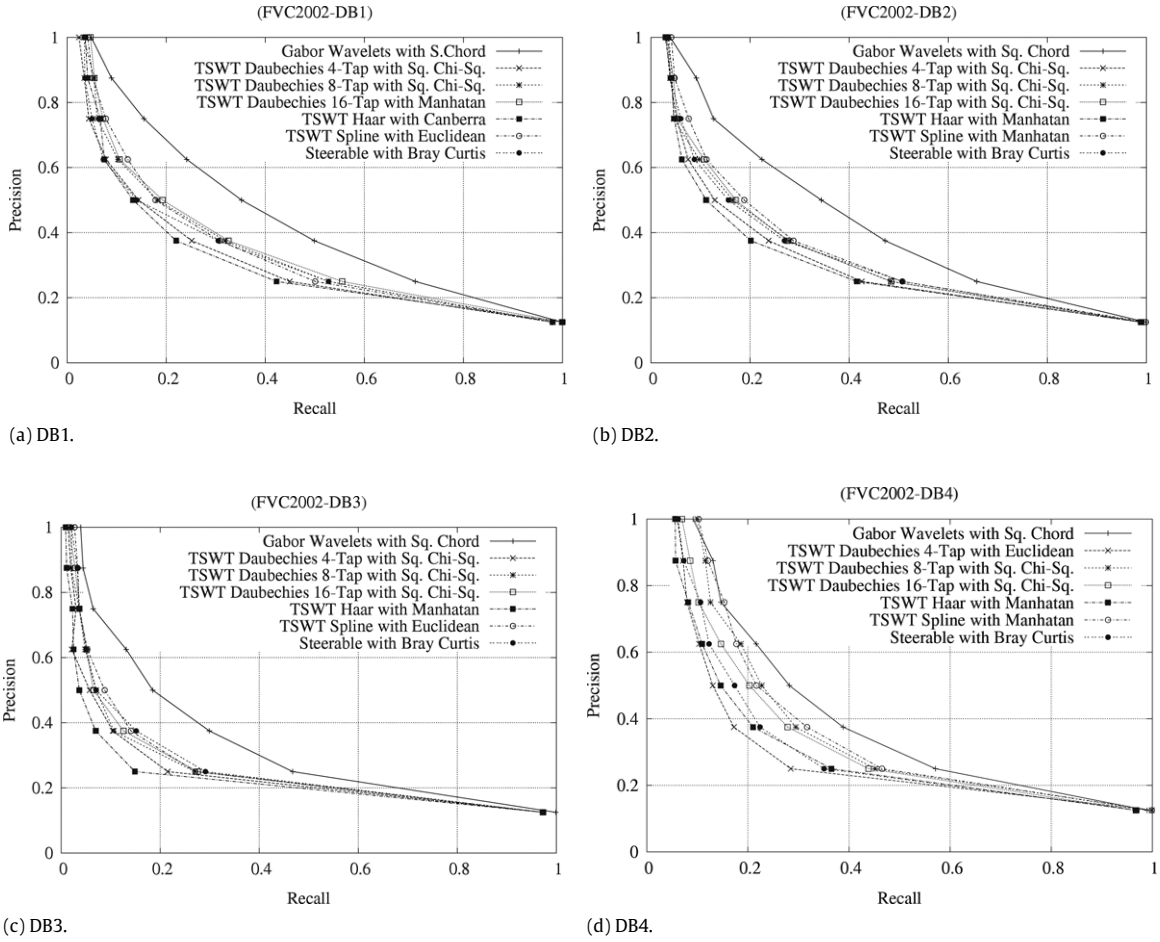

Fig. 5. Average precision vs. Recall curves for the FVC-2002 database.

9.2. Effectiveness evaluation

In order to compare the retrieval effectiveness of different types of wavelets, the proposed approach was measured in terms of precision and recall curves [38], since they have been widely used to evaluate retrieval effectiveness.

The precision is defined as the fraction of the retrieved images that are relevant to the given query, while the recall represents the proportion of relevant images among the retrieved ones. Thus, each of the retrieved images is considered as a match if it belongs to the same class as the query image. Considering the query image q and the number of correct, missed and false candidates (n_c, n_m, and n_f, respectively), the precision p_q in the first R retrieved images is defined as follows:

$$p_q = \frac{n_c}{n_c + n_f} = \frac{n_c}{R}, \tag{22}$$

while the recall r_q of the such similar candidates S of the query image q is defined as:

$$r_q = \frac{n_c}{n_c + n_m} = \frac{n_c}{S}. \tag{23}$$

9.3. Experiments

A series of experiments were conducted to test the retrieval accuracy of our fingerprint image retrieval system, using different wavelet-based feature extraction algorithms, and different similarity measures. The retrieval experiments were considered independently in each of the four data sets of the two databases.

A simulated query is one of the 880 images in the data sets. Thus, a total number of 880 different fingerprint queries were performed per data set. The relevant retrieved images for each query are defined as the remaining fingerprints from the same individual, and the distances between the images are stored in increasing order.

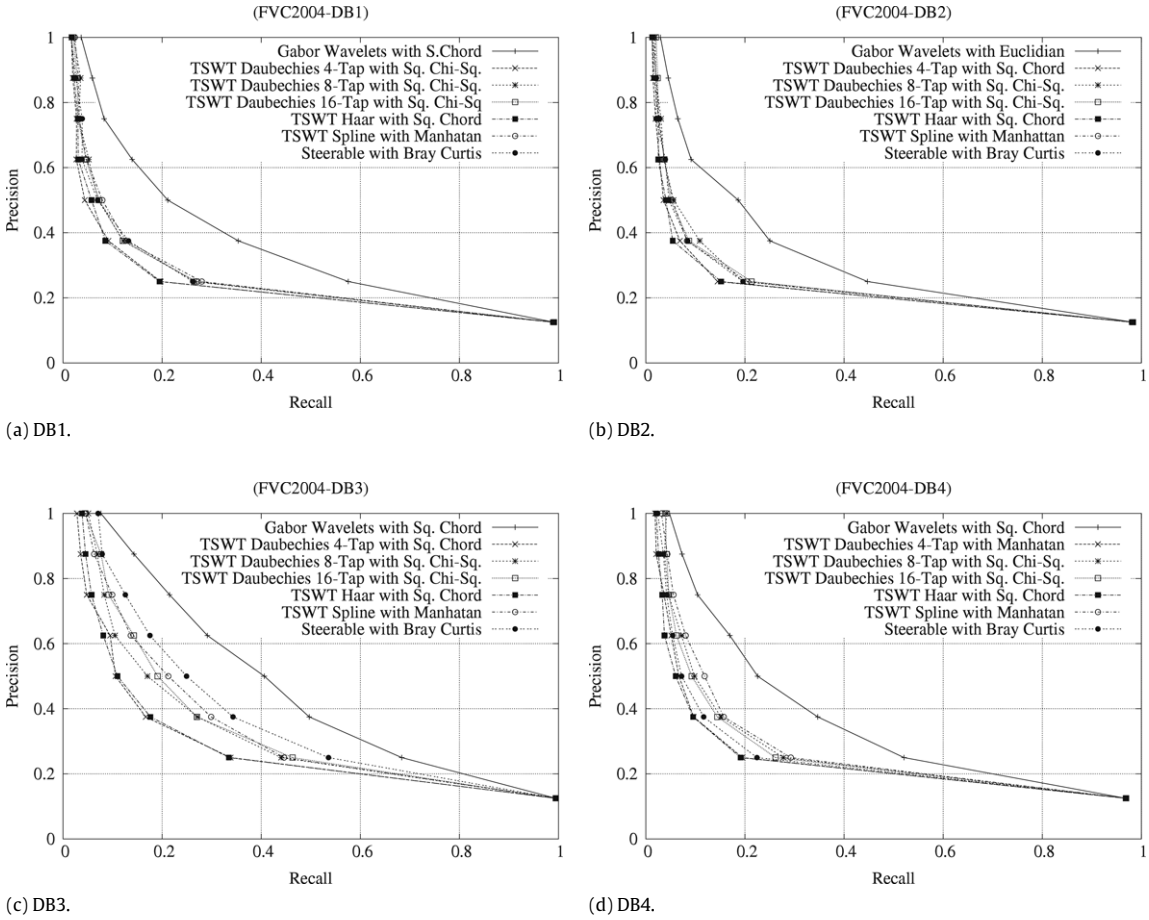

Fig. 6. Average Precision vs. Recall curves for the FVC-2004 database.

A total number of 42 image descriptors were tested in each data set to determine the best feature extraction algorithm and similarity measure pair. To generate them we have considered seven different wavelet-based feature extraction functions with the six similarity measures presented in Table 1. Seven different types of wavelets including Gabor wavelets, steerable pyramids, TSWD using Haar, Daub 4-tap, Daub 8-Tap, Daub 16-Tap, and spline wavelets have been evaluated.

Further, for each data set we have considered the average retrieval effectiveness of all 42 image descriptors. Thus, a total number of $42 \times 2 \times 4$ experiments were conducted. The best combinations are then found, and the precision vs. recall curves showing the accuracy of the image descriptors are presented in Figs. 5 and 6. Note that, for the sake of space, we report only the best results achieved by the image descriptors for each data set.

By considering both figures, it is clear that the Gabor wavelets outperform the other approaches in terms of retrieval accuracy. This is due to the fact that these wavelets capture much useful information at different orientations when compared with the traditional Tree-Structured Wavelet Decompositions which do not consider this specific information.

In all eight data sets the best accuracy of steerable pyramids was achieved by using the similarity measure based on the Bray Curtis distance. We can also observe that for each of the eight data sets, except for DB2 of the FVC-2004, the highest retrieval effectiveness was obtained by using the Square Chord similarity measure. The fact that the distance is first obtained by performing the square root of the feature values and then by applying the power of two operation emphasizes those features with large dissimilarity.

The retrieval accuracy obtained by the different types of TSWD is almost the same. The fact that this kind of wavelet does not capture much information at different orientations has decreased their effectiveness in comparison with the Gabor wavelets. The best similarity measure for the TSWD using spline wavelets are the Manhattan and Euclidean distances for both databases. That is because both of them measure the absolute differences in each feature dimension in order to increase the retrieval effectiveness. However, one benefit of the Manhattan distance is that it requires less computational operations than the Euclidean distance.

In the case of the TSWD using Haar wavelets, the best retrieval indices were obtained by using the Manhattan and Square Chord measures, whereas for the TSWD using Daubechies wavelets, the best retrieval effectiveness was achieved through the Square-Chi-Squared similarity measures. Note that the best retrieval effectiveness of the different types of the TSWD was

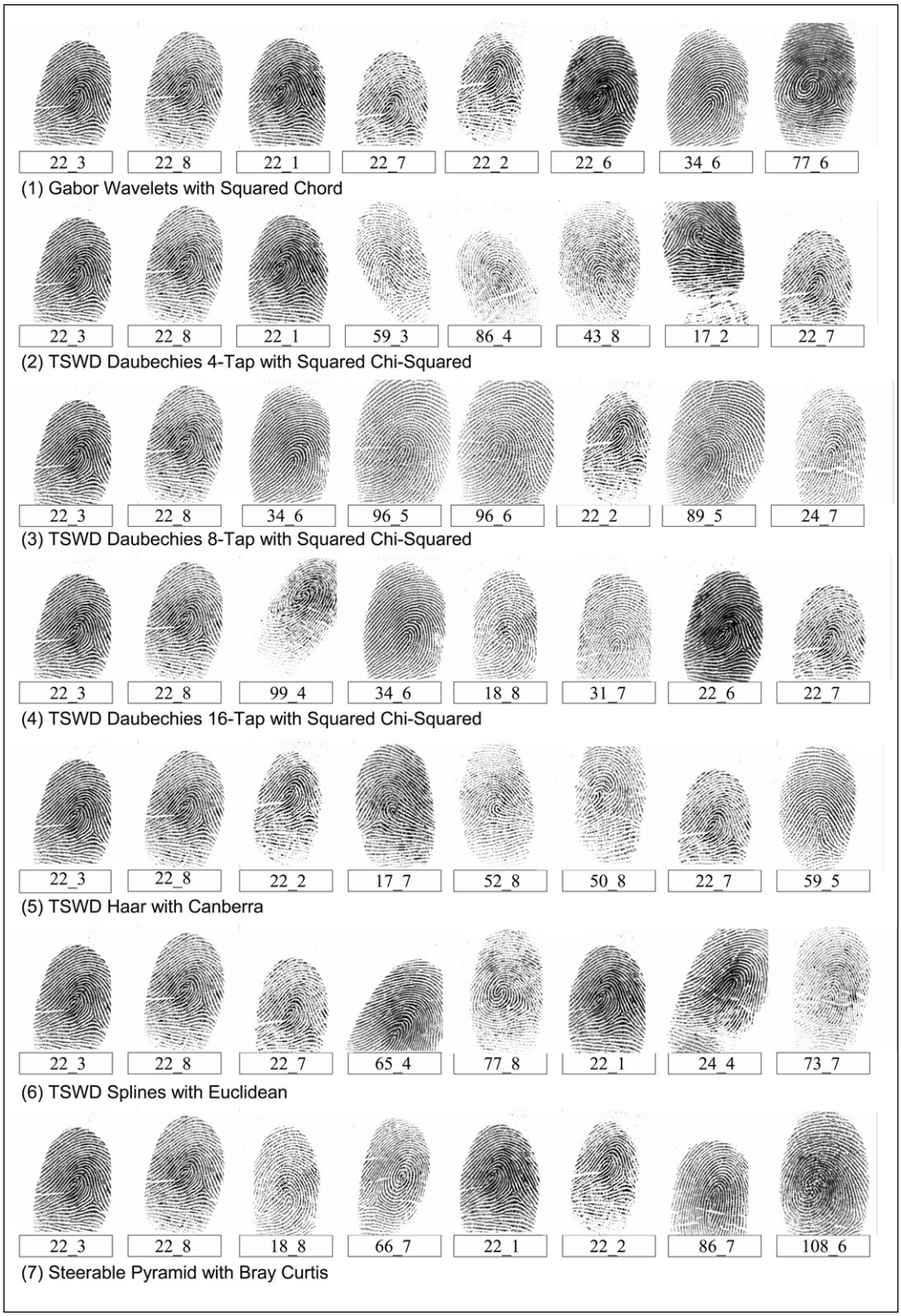

Fig. 7. Some retrieval examples of the data set DB1 of the FVC-2002 database.

obtained from the same similarity measures in both databases. This observation is important since the similarity measure used should have the same effectiveness for self class images.

9.4. Image retrieval examples

Some retrieval examples are shown in Fig. 7. The query image is on the top left corner, whereas the remaining ones are the retrieved images presented in increasing order of distance from the query image. Each fingerprint is labeled by the individual's ID and the number of the fingerprint sample, for example, image 22_3 will denote the individual number 22 and the third sample of his/her fingerprint. From Fig. 7, we can see that most of the retrieved fingerprints are visually similar to the query image. This observation is important because many of the errors on the retrieved data involve fingerprints that have the same texture and orientation as the query image, although they belong to other individuals. In other words, the presence of rotated or translated versions of similar fingerprints reduces the accuracy of the retrieval process.

10. Conclusions

This paper has investigated the possibility of applying texture-based image retrieval techniques to reduce the search space for fingerprint identification. More specifically, we have proposed a novel approach to characterize fingerprint images by using different types of wavelet transforms and similarity measures.

The retrieval effectiveness of the different image descriptors was compared by analyzing the results in terms of precision and recall curves. For all experiments, the best result was achieved by the Gabor Wavelet Transform combined with the Square Chord similarity measure. This fact relies basically on the flexibility of this type of wavelet to model the orientation and the scale information in images. Moreover, depending on the desired accuracy the descriptor parameter values can be adapted. The lack of this flexibility has influenced the retrieval performance of the Tree-Structured Wavelet Transform, since it is not able to capture relevant information at different orientations.

It is important to notice that the databases used in our experiments do not reflect real acquisition conditions in the sense that images present abnormal distortions, including noise, significant rotations, and translations [39]. In this context, future work includes the use of more realistic fingerprint image databases in which we expect that the retrieval effectiveness of our image descriptors will be considerably improved. Furthermore, we also plan to study the impact of using different metric access methods for fingerprint identification.

Acknowledgments

The first author was partially supported by the Brazilian National Council of Technological and Scientific Development — CNPq under grant # 134990/2005-6. This work was partially financed by CNPq, CAPES/COFECUB, FAEPEX, FAPESP, and supported by Microsoft eScience grant.

References

[1] A.K. Jain, A. Ross, S. Prabhakar, An introduction to biometric recognition, IEEE Transactions on Circuits and Systems for Video Technology 14 (1) (2004) 4–20.
[2] A.K. Jain, L. Hong, S. Pankanti, R. Bolle, An identity-authentication system using fingerprints, Proceedings of the IEEE 85 (9) (1997) 1365–1388.
[3] R.P. Wildes, Iris recognition: An emerging biometric technology, Proceedings of the IEEE 85 (9) (1997) 1348–1363.
[4] R.B. Hill, Retina Identification, Biometrics: Personal Identification in Networked Society, Kluwer Academic, 1999.
[5] W. Zhao, R. Chellappa, P.J. Phillips, A. Rosenfeld, Face recognition: A literature survey, ACM Computing Surveys 35 (4) (2003) 399–458.
[6] V.S. Nalwa, Automatic on-line signature verification, Proceedings of the IEEE 85 (2) (1997) 215–239.
[7] A. Eriksson, P. Wretling, How flexible is the human voice? — A case study of mimicry, Proceedings of EUROSPEECH 2 (1997) 1043–1046.
[8] B. Chiraz, C. R.G, D. L.S, Gait recognition using image self-similarity, EURASIP Journal on Applied Signal Processing 2004 (2004) 572–585.
[9] S. Pankanti, S. Prabhakar, A.K. Jain, On the individuality of fingerprints, IEEE Transactions on Pattern Analysis and Machine Intelligence 24 (8) (2002) 1010–1025.
[10] A.K. Jain, S. Prabhakar, S. Pankanti, On the similarity of identical twin fingerprints, Pattern Recognition 35 (11) (2002) 2653–2663.
[11] A.K. Jain, L. Hong, R.M. Bolle, On-line fingerprint verification, IEEE Transactions on Pattern Analysis and Machine Intelligence 19 (4) (1997) 302–314.
[12] W.T. Freeman, E.H. Adelson, The design and use of steerable filters, IEEE Transactions on Pattern Analysis and Machine Intelligence 13 (9) (1991) 891–906.
[13] T.S. Lee, Image representation using 2d gabor wavelets, IEEE Transactions on Pattern Analysis and Machine Intelligence 18 (10) (1996) 959–971.
[14] B.S. Manjunath, W.-Y. Ma, Texture features for browsing and retrieval of image data, IEEE Transactions on Pattern Analysis and Machine Intelligence 18 (8) (1996) 837–842.
[15] I. Daubechies, The wavelet transform, time-frequency localization and signal analysis, IEEE Transactions on Information Theory 36 (5) (1990) 961–1005.
[16] S.G. Mallat, A theory for multiresolution signal decomposition: The wavelet representation, IEEE Transactions on Pattern Analysis and Machine Intelligence 11 (7) (1989) 674–693.
[17] M. Unser, A. Aldroubi, M. Eden, A family of polynomial spline wavelet transforms, Signal Processing 30 (2) (1993) 141–162.
[18] C.T. Traina, A. Faloutsos, C. Seeger, Fast indexing and visualization of metric data sets using slim-trees, IEEE Transactions on Knowledge and Data Engineering 14 (2) (2002) 244–260.
[19] Fitz,Green, Fingerprint classification using a hexagonal fast fourier transform, Pattern Recognition 29 (10) (1996) 1587–1597.
[20] A.K. Jain, S. Minut, Hierarchical kernel fitting for fingerprint classification and alignment, ICPR 2 (2002) 469–473.
[21] Chong,Ngee,Jun,Gay, Geometric framework for fingerprint image classification, Pattern Recognition 30 (9) (1997) 1475–1488.
[22] Halici,Ongun, Fingerprint classification through self-organizing feature maps modified to treat uncertainties, Proceedings of the IEEE 84 (10) (1996) 1497–1512.
[23] L. Hong, A.K. Jain, Classification of fingerprint images, in: 11th Scandinavian Conference on Image Analysis, Kangerlussuaq, Greenland, 7–11 June, 1999.
[24] K. Karu, A.K. Jain, Fingerprint classification, Pattern Recognition 29 (3) (1999) 223–231.
[25] D. Maio, D. Maltoni, A structural approach to fingerprint classification, in: ICPR '96: Proceedings of the International Conference on Pattern Recognition, ICPR '96, IEEE Computer Society, Washington, DC, USA, 1996, pp. 578–585. Volume III-Volume 7276.

[26] R. Cappelli, D. Maio, D. Maltoni, L. Nanni, A two-stage fingerprint classification system, in: WBMA '03: Proceedings of the 2003 ACM SIGMM workshop on Biometrics methods and applications, ACM Press, New York, NY, USA, 2003, pp. 95–99.
[27] R.S. Germain, A. Califano, S. Colville, Fingerprint matching using transformation parameter clustering, IEEE Computational Science and Engineering 4 (4) (1997) 42–49.
[28] X. Tan, B. Bhanu, Y. Lin, Fingerprint identification: Classification vs. Indexing, in: Proceedings of the IEEE Conference on Advanced Video and Signal Based Surveillance, 2003, pp. 151–156.
[29] F. Wang, X. Zou, Y. Luo, J. Hu, A hierarchy approach for singular point detection in fingerprint images, in: Lecture Notes in Computer Science, 3072, 2004, pp. 359–365.
[30] A.K. Jain, S. Prabhakar, L. Hong, A multichannel approach to fingerprint classification, IEEE Transactions on Pattern Analysis and Machine Intelligence 21 (4) (1999) 348–359.
[31] K.-C. Liang, C.-C. Kuo, Waveguide: A joint wavelet-based image representation and description system, IEEE Transactions on Image Processin 8 (11) (1999) 619–1629.
[32] A. Natsev, R. Rastogi, K. Shim, Walrus: A similarity retrieval algorithm for image databases, IEEE Transactions on Knowledge and Data Engineering 16 (3) (2004) 301–316.
[33] C.K. Chui, An Introduction to Wavelets, Academic Press Professional, Inc., San Diego, CA, USA, 1992.
[34] T. Chang, C.-C.J. Kuo, Texture analysis and classification with tree-structured wavelet transform, IEEE Transactions on Image Processing 2 (4) (1993) 429–441.
[35] M.P. Paolo Ciaccia, P. Zezula, M-tree: An efficient access method for similarity search in metric spaces, in: 23rd International Conference on Very Large Data Bases, VLDB'97, 1997, pp. 426–435.
[36] R. Cappelli, D. Maio, D. Maltoni, A. Erol, Synthetic fingerprint-image generation, ICPR 03, 2000, p. 3475.
[37] R. Cappelli, D. Maio, D. Maltoni, Synthetic fingerprint-database generation, in: ICPR '02: Proceedings of the 16th International Conference on Pattern Recognition, ICPR'02, vol. 3, IEEE Computer Society, Washington, DC, USA 2002, p. 30744.
[38] W.I. Grosky, R. Jain, R. Mehrotra (Eds.), Handbook of Multimedia Information Management, Prentice-Hall, 1997.
[39] D. Maio, D. Maltoni, R. Cappelli, J.L. Wayman, A.K. Jain, Fvc 2002: Second fingerprint verification competition, in: Proceedings of the 16th International Conference on Pattern Recognition 2002, vol. 3, 2002, pp. 811–814.